Electron loss from 0.74- and 1.4-MeV/u low-charge-state argon and xenon ions colliding with neon, nitrogen, and argon

R. D. DuBois, A. C. F. Santos, and R. E. Olson
Department of Physics, University of Missouri–Rolla, Rolla, Missouri 65409, USA

Th. Stöhlker, F. Bosch, A. Bräuning-Demian, A. Gumberidze, S. Hagmann, C. Kozhuharov, R. Mann, A. Oršić Muthig, U. Spillmann, and S. Tachenov
Atomic Physics Division, GSI, 64291 Darmstadt, Germany

W. Barth, L. Dahl, B. Franzke, J. Glatz, L. Gröning, S. Richter, D. Wilms, and A. Krämer
Accelerator Division, GSI, 64291 Darmstadt, Germany

K. Ullmann and O. Jagutzki
Institüt für Kernphysik der J. W. Goethe Universität Frankfurt, Frankfurt am Main, Germany
(Received 18 April 2003; published 3 October 2003)

Absolute total-, single-, and multiple-electron-loss cross sections are measured for (Ar^{+}-, Ar^{2+}-, Xe^{3+})-(Ne, N_2, Ar) collisions at 0.74 and 1.4 MeV/u. In addition, a many-body classical trajectory Monte Carlo model was used to calculate total- and multiple-electron-loss cross sections for Ar^{+} impact. For N_2 and Ar targets, excellent agreement between the measured and calculated cross sections is found; for the Ne target the experimental data are approximately 40% smaller than the theoretical predictions. The experimental data are also used to examine cross-section scaling characteristics for electron loss from fast, low-charge-state, heavy ions. It is shown that multiple electron loss increased the mean charge states of the outgoing argon and xenon ions by 2 and 3 respectively. The cross sections decreased with increasing number of electrons lost and scaled roughly as the inverse of the sum of the ionization potentials required to sequentially remove the most weakly bound, next most weakly bound, etc., electrons. This scaling was found to be independent of projectile, incoming charge state, and target. In addition, the experimental total loss cross sections are found to be nearly constant as a function of initial projectile charge state. As a function of impact energy, the theoretical predictions yield an $E^{-1/3}$ behavior between 0.5 and 30 MeV/u for the total loss cross sections. Within error bars, the data are consistent with this energy dependence but are also consistent with an $E^{-1/2}$ energy dependence.

DOI: 10.1103/PhysRevA.68.042701 PACS number(s): 34.50.Fa

I. INTRODUCTION AND BACKGROUND

Electron loss, also referred to as projectile ionization or stripping, is an important ionization component in dressed ion-atom collisions. It increases the charge state of the projectile and liberates fast electrons to the continuum. Often projectile ionization is associated with simultaneous ionization of the target. Electron loss plays a major role in stopping power and energy deposition by fast ions, particularly for energies around a few hundred keV/u; it provides an excellent testing ground for enhancing our knowledge of many-body atomic processes since the number of interacting particles can be controlled simply by the choice of ion and charge state. It is a primary tool in accelerating ion beams to high energies, and is important in neutron-induced radiation damage of tissue since this is how charged ions are produced from neutral recoil fragments generated by neutron bombardment. Electron-loss studies can also be used to provide information about ionization of an ion by the combined Coulomb forces of a partially screened target nucleus and its bound electrons.

For these reasons, there exists a long history of electron-loss experiments, beginning in 1920s when Rutherford measured stopping power for α particles passing through air [1]. During the period from 1960s to 1980s, a multitude of studies were performed, in part to study the fundamental atomic processes themselves but also in order to extract experimental parameters used to accelerate ions to higher and higher energies. Since that time, additional experiments have investigated multiple-ionization processes and scaling behaviors. For compilations and selected examples of experimental information available, see Refs. [2–15].

On the theoretical side, projectile ionization resulting from collisions with neutral targets is a complex, many-body process. Further complications are that projectile ionization results from interactions with both the partially screened target nucleus and the bound target electrons, the relative importance of these channels varies with impact energy, the amount of screening depends on the number of projectile electrons removed, and the number of target electrons actively involved depends not only on the impact energy but also on which projectile electrons are being removed, i.e., both on the initial projectile charge plus the number of electrons removed. As a result, few theoreticians have tackled this difficult subject even though the basic methods were outlined many years ago [16].

In spite of this, in 1948 Bohr [17] used semitheoretical arguments and predicted a v^{-1} dependence for stripping of light particles by intermediate Z targets, in accordance with the dependence found by Rutherford in his stopping-power

measurements. More recently, Montenegro and Meyerhof [18] have performed calculations for relatively few electron systems. For the many-body systems of interest here, Shevelko and Olson have calculated electron-loss cross sections using two different approaches. Shevelko used a nonrelativistic Born model to calculate cross sections, and then scaled his results to account for ionization of the projectile by the partially screened target nucleus and target electrons. Using this approach he calculated total loss cross sections and beam storage lifetimes at high energies for a variety of projectiles interacting with gases [19–21]. Olson used a many-body classical trajectory Monte Carlo treatment to calculate single- and multiple-loss cross sections [15,22]. Although both methods were demonstrated to be in agreement with selected sets of experimental data, differences between them are that the CTMC method included multiple electron removal processes whereas the Born treatment only incorporated single-electron transitions. The scaled Born approximation predicts an E^{-1} energy dependence at higher energies whereas the CTMC method predicts a much slower dependence.

In spite of decades of research and the large database of electron-loss information available, except for the lightest projectiles, existing data are limited to impact energies less than approximately 200 keV/u. For heavier projectiles, some data exist in the MeV/u range, but only for highly stripped ions. This lack of information for fast, low-charge-state, and heavy ions is particularly relevant because electron-loss cross sections have recently become major questions relating to large projects under way in the USA and Germany. Both projects require intense beams of heavy ions having energies of tens to hundreds of MeV/u. In the USA, the impetus is the heavy-ion fusion program where it is proposed to bombard a deuterium-tritium (DT) pellet with intense beams of heavy, singly charged ions; the goal being to achieve laboratory fusion. In Germany, a planned upgrade of the accelerators at the GSI-Darmstadt requires acceleration of heavy ions with low-charge states to relativistic energies, one reason being future studies of nuclear processes involving radioactive species lying far from the stability curve.

In both cases, intense beams must be accelerated and transported through long distances. Interactions with background gases in the beamline lead to energy and charge straggled beam components. Loss of these components is highly detrimental as it not only decreases the beam luminosity, it also can contribute to erosion of the vacuum walls and lens elements, and can lead to radiation buildup via activation of components in the beamline; additionally, due to localized heating and desorption along the beamline the background pressures increase, further amplifying the problems. These problems can be reduced to acceptable values by lowering the overall vacuum, but at a considerable expense. In the worst case, additional improvements in the vacuum may be technologically infeasible.

In addition, the USA project requires both high beam intensity and a tight focus on the target to achieve the necessary power density to induce fusion. This means minimizing space-charge blowup effects by using low-charge-state beams. Electron loss in the poor vacuum of the reaction chamber containing the DT pellet increases the mean charge state of the beam, which increases the focal spot size and decreases the power density on the target. At GSI, the high-energy beams will be injected into synchrotrons and accelerated to 100-MeV/u energies. Loss processes in the rings may reduce the final beam intensities and luminosities available for experiments. In addition, loss processes lead to reduced storage lifetimes, again restricting what physics can be investigated. The reader is referred to Refs. [23] and [24] for additional details on these projects.

Spurred by these needs for electron-loss information at MeV/u energies and for low-charge-state ions, several experiments were performed at the Texas A&M University. In one case [15], electron loss from Xe^{18+} was measured between 2 and 10 MeV/u. In other work [25], data were collected using selected charge states (Ar^{6+} and Ar^{8+}) and impact energies (10.2 and 19 MeV/u). However, neither of these experiments addresses the question of loss from very low charge state or singly charged ions, nor do they test theoretical predictions for singly charged ions.

Therefore, in collaboration with the University of Missouri–Rolla and the Atomic Physics and Accelerator groups at the GSI-Darmstadt, a systematic investigation of electron loss from low-charge-state heavy ions interacting at high energies with various gases was initiated. Here, we report absolute cross sections measured at 0.74 and 1.4 MeV/u for single and multiple electron loss from Ar^{+}, Ar^{2+}, and Xe^{3+} ions colliding with neon, argon, and molecular nitrogen targets. These data provide information about the relative importance of multiple-loss processes, as well as information about how the cross sections scale as a function of incoming projectile charge state, impact energy, and target Z. In addition, these data provide an opportunity to test the many-body CTMC calculations for systems containing many, loosely bound, electrons.

II. EXPERIMENTAL METHOD AND PROCEDURES

The measurements were performed at the GSI UNILAC using the gas stripper as a target and the beam transport analyzing magnet as a postcollision charge state analyzer. Post-collision charge state intensities were measured by inserting a high-rate position sensitive detector immediately behind the analyzing magnet and using a fast histogramming time-to-digital converter and PC to collect data. (The time structure of the beam, e.g., 3 Hz at 1 ms with a duty cycle of 0.3%, precluded using standard list-mode methods.) Slits inserted before and after the gas stripper were used to define the beam axis, collimate and reduce the beam intensity, and to define the beam divergence. These slits also provided differential pumping between the target and accelerator/detector regions. By valving off the high-speed pumps normally used to pump the gas target and opening the leak valve to the gas jet, a pseudostatic gas target filling the gas target chamber between the entrance and exit slits was formed. The target pressure at the periphery of the chamber was measured with an ion gauge.

The experimental procedure consisted of accelerating argon, xenon, and helium ion beams to energies ranging from

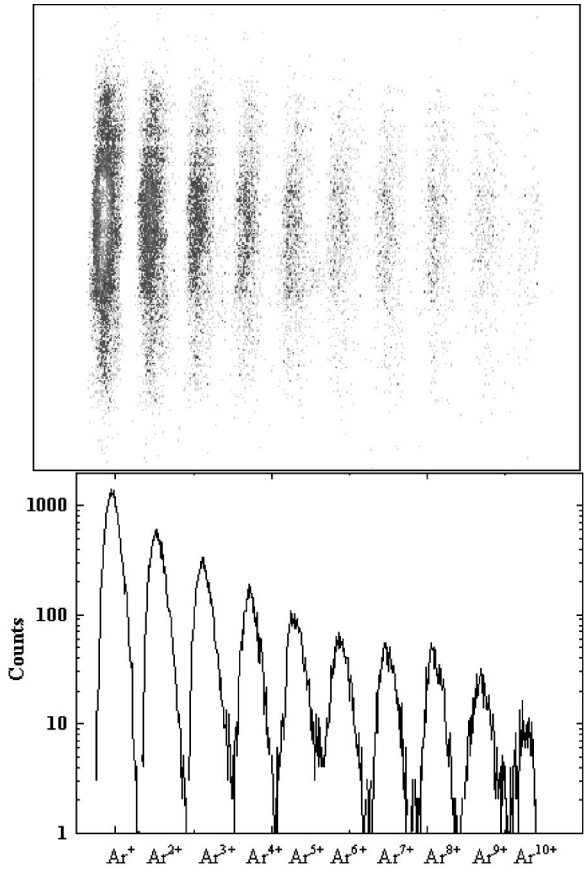

FIG. 1. Top figure: two-dimensional spectrum of the post-collision charge states for 0.74-MeV/u Ar^+ impact on Ar. Bottom figure: one-dimensional projection of the above spectrum.

0.74 to 1.4 MeV/u, passing them through the target region, and measuring the postcollision charge state spectra as a function of target pressure, i.e., the growth curve method. For each energy and beam the intensity had to be reduced by many orders of magnitude in order to perform the experiment. Therefore, efforts were made to reduce the intensity in a manner that uniformly illuminated the entrance slit and to ensure that the beam was centered on the slit. Counting rates were typically 100 kHz, which, by further decreasing the beam intensity, were shown to be well within the capabilities of the detector, electronics, and histogramming time-to-digital converter.

A typical two-dimensional (2D) spectrum, shown in Fig. 1, illustrates well-separated islands for the various charge states and small background intensities between the islands. The lower part of the figure shows a projection of these data to generate a 1D charge state spectrum. Either the 2D or the 1D spectra could be integrated and used to determine the charge state intensities. For loss from Xe^{3+}, the number of electron-loss channels having significant intensity is larger than for argon projectiles. Therefore, for xenon, one-dimensional charge state spectra were fitted with a polynomial background and Gaussian peaks to extract the charge state
intensities.

To convert the target pressures measured at the periphery of the target chamber to absolute target thicknesses along the

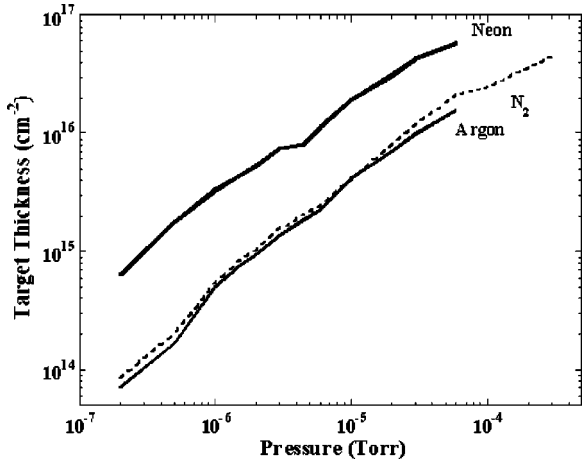

FIG. 2. Effective target thicknesses as a function of gas pressure measured at the periphery of the target chamber. Thicknesses were calibrated using known cross sections and measured charge state fractions for 0.74-MeV/u He^+ impact, as described in the text.

beam path (target density times path length), the following calibration procedure was used. For each target gas, growth curves were measured for electron capture and loss by 0.74-MeV/u He^+ ions. Using known absolute cross sections for ionization, capture, and loss by He, He^+, and He^{2+} impact [3,26–31], charge state fractions as a function of target density were calculated for each target. Then, by comparing the measured and calculated values, conversion tables between measured pressure and effective target thickness were determined. The results are shown in Fig. 2. In performing this calibration, it was demonstrated that the uncertainties in the target thickness primarily depended on and were directly proportional to uncertainties in the absolute single-electron-loss cross sections for He^+ impact. From overlaps or extrapolation between cross sections measured by different groups, the published cross sections used in this calibration procedure were assigned an absolute accuracy of $\pm 30\%$.

Next, postcollision charge state intensities were measured as a function of target thickness for each projectile, impact energy, and target. Typically, data accumulation times were such that a total of 10^5 counts were accumulated and target pressures were varied from base vacuum to a maximum value where electron loss decreased the main beam intensity by approximately 20–30 %. Background subtracted intensities for the various charge states were determined and converted to charge state fractions. In calculating the fractions, it was assumed that at the high beam energies employed here, all charge states were detected with the same efficiency. The measured fractions were plotted versus target density, generating growth curves similar to those shown in Fig. 3.

Absolute electron-loss cross sections were extracted by using the linear term of polynomial fits to the measured growth curves. Typically, a second-order polynomial provided an adequate fit; third-order polynomials were also used in certain cases. To check whether, and to what extent, multiple collisions influenced the cross sections for the loss of many electrons in a single collision, the following method was used. In a single collision, a particular charge state q can

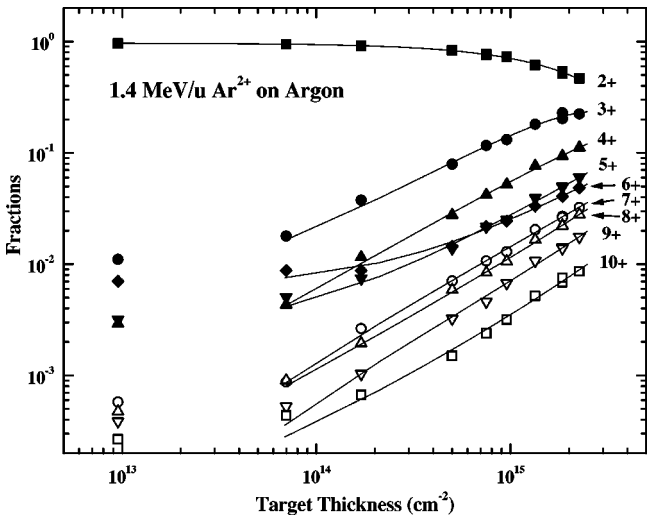

FIG. 3. Postcollision charge state fractions measured as a function of target thickness for 1.4-MeV/u Ar^{2+}-Ar collisions. Solid lines are polynomial fits to data.

be generated by single- and multiple-electron capture or loss from higher and lower charge states q'. Thus, the charge state fractions are related by

$$F_q(\pi) = \sum_0^\infty \pi F_{q'}(\pi)\sigma_{q',q}. \quad (1)$$

Here $F_q(\pi)$ is the measured fraction for charge state q at target density π and $\sigma_{q',q}$ is the cross section for the projectile going from charge state q' to charge state q. The sum is over all possible charge states generated in previous collisions. By using the fractions measured at several target densities, it is possible to generate and solve a matrix of coupled equations and extract cross sections for single-collision transitions from the initial to final charge state. This was done for three cases, namely, when the equations include sums over the two, three, or four dominant channels, i.e., q_{in}, $q_{in}+1$, $q_{in}+2$, $q_{in}+3$, listed in order of declining importance. By comparing cross sections obtained for these three cases with those determined from our polynomial fits, it was found that single-collision conditions generally dominated except for a few cases involving loss of many electrons. In those cases, the matrix equation results were averaged and this average value used; when single collisions dominated, the matrix equation and polynomial fit results were all averaged together.

Hence, uncertainties in the absolute cross sections presented here are a combination of uncertainties associated with the target thickness calibration, uncertainties associated with the extraction of cross sections from the data, and statistical uncertainties. These are taken to be $\pm 30\%$, less than 5%, and less than 10%, respectively. For selected cases involving the loss of many electrons where the cross sections are small, contamination of the incoming beam due to charge changing collisions in the beamline becomes important. This limits the accuracy of the cross sections that can be extracted; hence factors of 2 or larger uncertainties are possible. It should also be noted that the total loss cross sections shown in the figures and table were obtained by fitting the decay curve for the main beam with an exponential. These values typically agreed with the sum of the single- and multiple-loss cross sections within about 15–20 %, which is another indication of the overall accuracy of the data and fitting procedures.

III. RESULTS

Using the methods outlined above, absolute cross sections were measured for total, single, and multiple projectile electron loss for 0.74-MeV/u Ar^+ and 1.4-MeV/u Ar^+, Ar^{2+}, and Xe^{3+} ions colliding with neon, molecular nitrogen, and argon targets. Single- and multiple-electron-loss cross sections, plotted as a function of the number of electrons lost, are shown in Fig. 4 and along with this, the total loss cross sections are tabulated in Table I. For comparison purposes, the cross sections for the nitrogen target have been divided by 2 in order to compare data for a series of ''atomic'' targets. The error bars associated with the total loss cross sections represent the total absolute uncertainties associated with each collision system. These total uncertainties are primarily due to uncertainties in the target thickness calibration. The larger uncertainties for the (Ar^+-, Xe^{3+})-Ne data are associated with reproducibility between different datasets. For the single- and multiple-loss cross sections, the error bars are due to uncertainties in fitting the data or solving the coupled equations. Total uncertainties for the single- and multiple-loss data would be a combination of the fitting uncertainties and the uncertainties in target thickness.

These data demonstrate two things. First, the total loss cross sections are large, roughly geometrical in size, and second, multiple-loss processes are important for these fast, low-charge-state ions. As seen, for Ar projectiles the cross sections decrease only by a factor of 2–2.5 for the removal of each additional electron, and for Xe the decrease is even slower. Therefore multiple loss accounts for roughly half of the total loss cross section in all cases, i.e., theoretical treatments must account for multiple electron removal processes. It should be noted that this behavior is in accordance with *n*-body CTMC (*n*CTMC) calculations in Ref. [22]. Also note that a change in slope in the cross sections can be observed in the vicinity where three or four electrons are lost. Assuming sequential removal of the most weakly bound outermost electrons, this change in slope roughly corresponds with the onset for removal of electrons from the next innermost subshell, i.e., the *s* shell which would open after the remaining three, four and five *p* electrons are removed from Xe^{3+}, Ar^{2+}, and Ar^+ respectively.

Also note the similar shapes of the curves. This implies that, except for absolute magnitude, the loss cross sections are independent of target. To test this, ratios were calculated for the neon and nitrogen targets divided by the corresponding cross sections for an argon target. It was found that the ratios were generally independent of impact energy and projectile species. On the average, for loss of up to six electrons, the cross sections induced by collisions with neon and nitrogen atoms were roughly 45% and 65% of those induced by

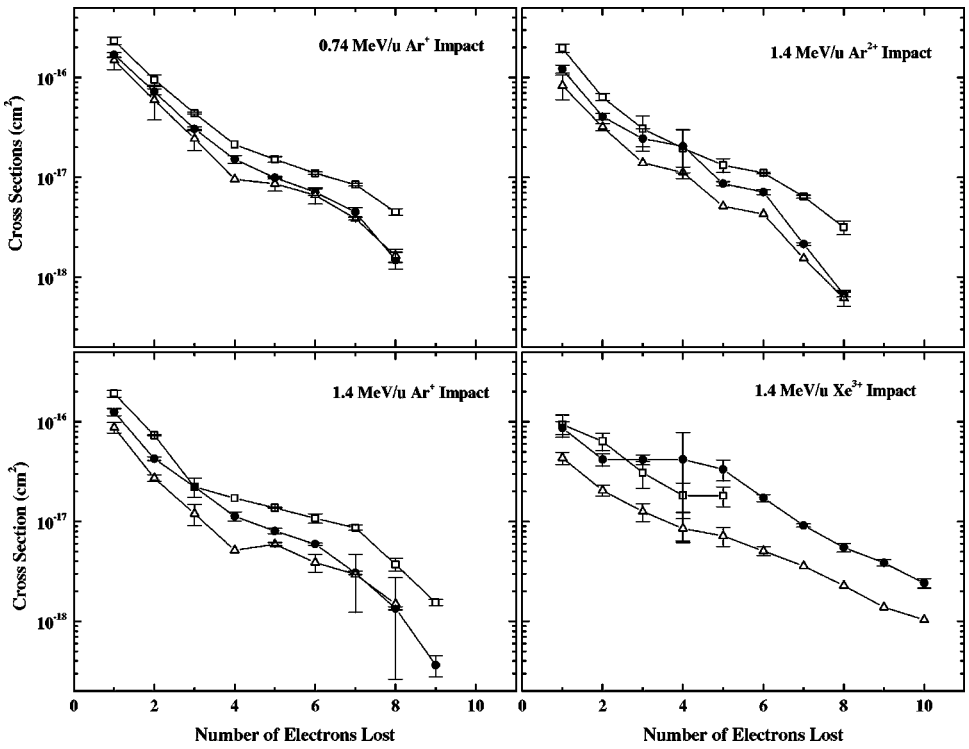

FIG. 4. Absolute cross sections for single- and multiple-electron loss for 0.74 and 1.4-MeV/u impacts on neon (open triangles), molecular nitrogen (closed circles), and argon targets (open squares). The molecular nitrogen cross sections have been divided by 2 in order to simulate cross sections for an atomic nitrogen target. The error bars shown for single and multiple electron loss represent relative uncertainties associated with statistics and cross-section extraction uncertainties.

argon. For higher degrees of projectile ionization, the efficiency of ionization by argon targets steadily increases. In other words, different targets were found to influence the magnitude but not the shape of single- and multiple-loss cross sections.

The average number of electrons lost per collision was calculated. Independent of initial charge state, impact energy, and target, it was found that on the average two electrons are lost from the argon projectiles whereas approximately three are lost from xenon. In other words, the mean charge states of these beams increase by 2 and 3 as they traverse tenuous targets of neon, nitrogen, and argon. For comparison, we note that on the average for 2–9 MeV/u Xe^{18+} ions passing through nitrogen [15], two electrons are lost, and that this number systematically decreased with increasing impact energy.

In Fig. 5 the multiple-loss cross sections are plotted versus the energy required to sequentially remove the most loosely bound electrons, i.e., versus ΣV_{ion}, the sum of the ionization potentials. It is seen that the cross sections scale roughly as $(\Sigma V_{\mathrm{ion}})^{-1}$; fits to the data yield a dependence of $(\Sigma V_{\mathrm{ion}})^{-1.1}$. Figure 5 demonstrates that this scaling is independent of projectile type, initial charge state, and impact energy. A similar dependence was noted in calculated cross sections for 2–20 MeV/u Xe^{i+} $(i=1-18)$ colliding with molecular nitrogen [15].

TABLE I. Absolute cross sections for total-, single-, and multiple-electron loss for 0.74 and 1.4-MeV/u impact on Ar, N, and Ne targets. The molecular nitrogen cross sections have been divided by 2 in order to simulate cross sections for an atomic nitrogen target. All the cross sections are in 10^{-16} cm^2. Numbers in parentheses are total percentage uncertainties for total cross sections.

Energy	0.74 MeV/u			1.4 MeV/u								
Projectile/target	Ar^+/Ar	Ar^+/N	Ar^+/Ne	Ar^+/Ar	Ar^+/N	Ar^+/Ne	Ar^{2+}/Ar	Ar^{2+}/N	Ar^{2+}/Ne	Xe^{3+}/Ar	Xe^{3+}/N	Xe^{3+}/Ne
Total loss	4.84	2.91	2.07	4.03	2.10	1.73	3.37	2.20	1.87	2.82	2.41	1.08
	(30)	(30)	(30)	(30)	(30)	(47)	(30)	(30)	(30)	(33)	(30)	(55)
1 loss	2.35	1.69	1.49	1.92	1.25	0.876	1.97	1.22	0.833	0.938	0.871	0.435
2 loss	0.952	0.724	0.596	0.733	0.428	0.273	0.636	0.407	0.320	0.640	0.420	0.206
3 loss	0.442	0.307	0.244	0.224	0.224	0.120	0.308	0.245	0.140	0.309	0.418	0.126
4 loss	0.214	0.152	0.0959	0.172	0.113	0.0518	0.197	0.206	0.112	0.183	0.422	0.0855
5 loss	0.152	0.0997	0.0864	0.138	0.0808	0.0594	0.133	0.0868	0.0515	0.182	0.334	0.0719
6 loss	0.110	0.0714	0.0666	0.108	0.0596	0.0391	0.111	0.0713	0.0429		0.173	0.0509
7 loss	0.0849	0.0449	0.0387	0.0869	0.0306	0.0297	0.0642	0.0215	0.0154		0.0915	0.0359
8 loss	0.0450	0.0149	0.0165	0.0373	0.0135	0.0150	0.0317	0.0067	0.0062		0.0551	0.0228
9 loss				0.0155	0.0037						0.0387	0.0139
10 loss											0.0243	0.0104

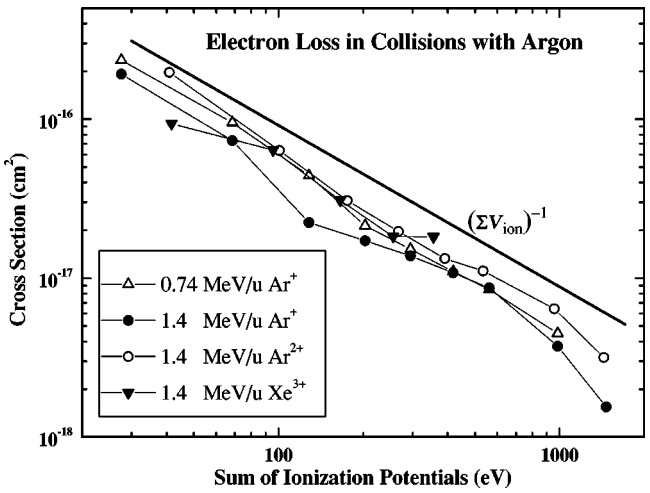

FIG. 5. Single- and multiple-electron-loss cross sections for collisions with argon. The cross sections are plotted vs the sum of the ionization potentials (ΣV_{ion}) required to remove the outermost electron in a sequential fashion. The solid line illustrates a $(\Sigma V_{\mathrm{ion}})^{-1}$ dependence.

Two of the primary goals of this experiment were to investigate the velocity dependence for electron loss by fast, low-charge-state, heavy ions and to provide benchmark cross sections for testing theoretical predictions. Regarding the velocity dependence, as mentioned in Sec. I, Born theories based on single-electron transitions predict a E^{-1} dependence at high energies, whereas CTMC calculations which incorporate multiple-electron transitions yielded a v^{-1} dependence for loss from Xe^{18+} ions [15].

In Fig. 6, measured and calculated total loss cross sections are shown for Ar^+ colliding with Ar, N_2, and Ne. Again, the measured N_2 data are divided by 2 in order to compare with the calculations done for an atomic target. In addition, the nitrogen and neon curves have been shifted for display purposes. The calculated cross sections are from an *n*CTMC

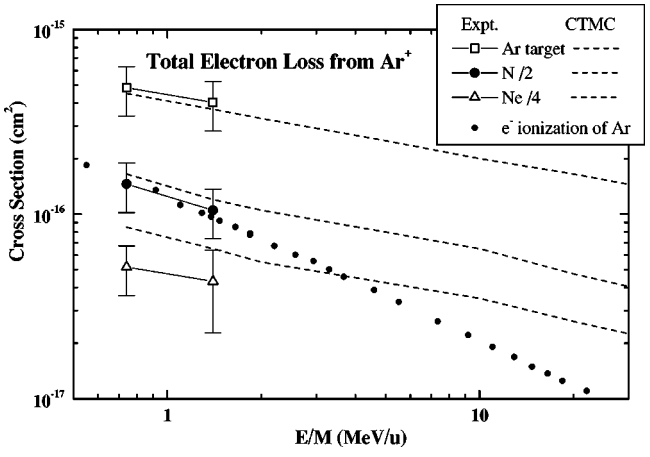

FIG. 6. Measured and calculated total electron-loss cross sections for (Ar^+)-(Ne, N, Ar) collisions as a function of impact energy. The N and Ne target data have been shifted for display purposes. The small squares for electron-impact ionization of argon are from Ref. [32]

model that has been outlined in Ref. [15]. For total loss induced by interactions with argon and nitrogen, the agreement between experiment and theory is very good, both in magnitude and velocity dependence; for the neon target, the experimental data are roughly 40% smaller in magnitude than the calculated values. Overall, within error bars, the experimental data are in accordance with a v^{-1} dependence. Although not shown, within uncertainties the experimental single-loss cross sections also demonstrate a v^{-1} dependence. As mentioned, a v^{-1} dependence was found experimentally in the 5–10 MeV/u range for electron loss from Xe^{18+}; at lower energies approaching those of the present work, a slower dependence was found [15]. However, the present CTMC calculations clearly have a slower decrease with energy (namely, on the order of $E^{-1/3}$), which, for the limited energy range investigated, is also in accordance with the experimental data.

In Fig. 6 our total electron-loss cross sections are also compared to electron-impact ionization data. The electron-impact cross sections are the sum of single and multiple cross sections for electron-impact ionization of argon [32]. For 1 keV electron impact, the single-ionization cross sections of Ar are a factor of 2 larger than for ionization of Ar^+ [33]. We make this comparison with electron impact since electron loss from Ar^+ ions occurs due to the combined Coulomb fields of the target electrons and screened nuclear charge Z_{eff}. Therefore at high impact energies where electron- and proton-impact ionization cross sections are identical, the target can be considered to consist of an effective number of electrons, N_{eff}, where $N_{eff} \leqslant Z_{eff}^2 + N$. Here N is the total number of electrons of the electron-loss collision partner. Thus, in lowest order, the electron-loss cross section can be obtained by multiplying the electron-impact cross sections by N_{eff}. Comparing the cross sections for electron loss from Ar^+ and impact ionization of Ar at 0.74 and 1.4 MeV/u, we find that N_{eff} is approximately 1.5, 2, and 3 for Ne, N, and Ar, respectively. Compared to electron-impact ionization of Ar^+, the values would be twice as large. Thus, a nitrogen atom appears to be equivalent to only four free electrons with regard to stripping of a MeV/u Ar^+ ion.

Our main purpose for making this comparison, however, is to provide information about electron loss in the tens of MeV/u region. We emphasize that using normalized electron-impact cross sections provides a lower estimate of the electron-loss cross sections. This is because (a) electron-impact ionization data have a $\log_{10}E/E$ energy dependence at high energies, whereas electron-loss data tend to demonstrate a slower energy behavior, and (b) it is well known that multiple electron loss from heavy ions is very important, even at high energies, whereas multiple target ionization is much less important. Both of these imply increasing deviation between electron-impact and electron-loss cross sections at higher and higher energies. Keeping this in mind, as shown in Fig. 6, for 25-MeV/u Ar^+ ions interacting with nitrogen atoms, a lower limit for the total electron-loss cross section is 2×10^{-17} cm^2 (note that the N target data are shifted downwards by a factor of 2). This value is about a factor of 4 smaller than what is predicted by CTMC calculations, the

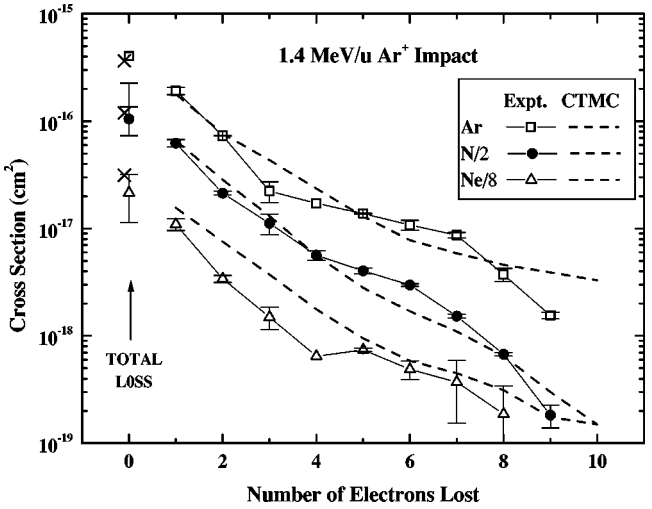

FIG. 7. Measured and calculated cross sections for single- and multiple-electron loss from 1.4-MeV/u Ar^+ colliding with Ne, N, and Ar. The N and Ne target data have been shifted for display purposes. CTMC total cross sections are indicated by crosses.

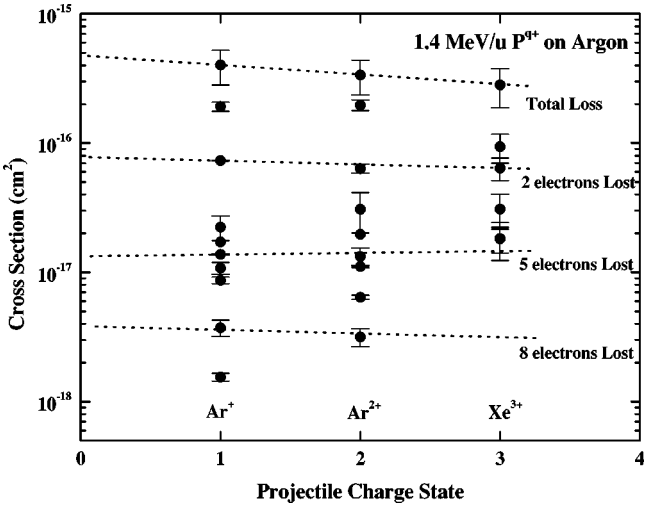

FIG. 8. Cross sections for electron loss from 1.4-MeV/u ions colliding with argon. The dotted curves serve only to guide the eye.

difference primarily arising from a v^{-1} versus a $\log_{10}E/E$ energy dependence.

In Fig. 7, an additional test of theory is made. Here, measured cross sections for total and multiple (up to ten) electron loss from Ar^+ are compared with CTMC calculations. Overall, extremely good agreement is found, although for collisions with neon, the experimental data are smaller than the theoretical values. This may be associated with experimental uncertainties as the measured cross sections for a neon target are also smaller than those measured for a ''lighter'' target, namely, nitrogen.

Also of interest is how the cross sections scale with initial projectile charge. For stripping of xenon ions in collisions with nitrogen targets for impact energies between 2 and 20 MeV/u, the CTMC model predicted that for Xe^+–Xe^{3+} projectiles, the cross sections would only decrease by approximately 20–40 % [15]. For higher incoming charge states, the cross sections were predicted to decrease roughly as q^{-1}. In Fig. 8 we plot the cross sections for 1.4 MeV/u ions colliding with argon. The xenon data were included in order to look at the q dependence over a broader range. Lines drawn through the data are simply to guide the eye. Here, the total loss cross sections demonstrate a slow decrease with increasing projectile charge while some of the multiple-loss cross sections actually increase in magnitude with increasing projectile charge. Overall, a general statement consistent with all the total- and multiple-loss cross sections and for all the targets investigated in this work is that within experimental uncertainties no cross-section dependence on the incoming charge state was found for the limited range of low-charge states investigated here. This also indicates that the cross sections for ionization of Ar and Ar^+, as were compared in Fig. 6, should not be too different.

IV. CONCLUDING STATEMENTS

Absolute cross sections for total, single, and multiple loss were presented for 0.74- and 1.4-MeV/u low-charge-state argon and xenon ions colliding with several targets. These measurements for electron loss from very low-charge-state heavy projectiles in the MeV/u range greatly extend the energy range of existing electron-loss data. By judicially selecting the collision systems, we were able to investigate cross-section systematics. First, these data demonstrated that independent of impact energy, target, or projectile species, the mean charge state of the argon and xenon ions increased by 2 and 3 respectively. Second, again independent of impact energy, target, or projectile species, the multiple-loss cross sections were found to scale roughly as $(\Sigma V_{\text{ion}})^{-1}$. Third, the experimental data were compared to n-body CTMC calculations, and the accuracy of the theoretical calculations for these rather complex collision systems was confirmed. Fourth, the impact energy dependence was investigated. The theoretical predictions for an Ar^+ projectile yielded an $E^{-1/3}$ impact energy behavior; experimentally, either a $E^{-1/2}$ or a $E^{-1/3}$ was consistent with the data. Fifth, the total loss cross sections were found to be nearly constant for these low-charge-state ions, even though the number of available projectile electrons is decreasing and the energy required to remove them is increasing.

Pertaining to the heavy-ion fusion program, these experimental data and CTMC calculations imply that for 20-MeV/u low-charge-state ions traversing a reaction chamber where the pressure is 1 mTorr, between 36% and 58% of the beam will change its charge state for each meter of distance traveled and that this portion of the beam will increase its mean charge state by 2 or 3. Which percentage is correct depends on whether an $E^{-1/2}$ or an $E^{-1/3}$ energy dependence is used for extrapolation purposes. Relating to beam storage at high energies, in a 1×10^{-11} Torr vacuum, roughly 3.6 and 1.7×10^{-9} of a 100-MeV/u beam will change charge state per meter traveled, again depending on which energy dependence is used. This is roughly equivalent to losing somewhere between a third and a sixth of the beam for each second of storage time.

Finally, it should be pointed out that although no concrete reasons can be found, there are several indications that the

experimental values for collisions with neon may be too small in magnitude. One indication is that when comparing experiment to CTMC calculations, very good agreement is found for argon and nitrogen targets, whereas for neon a discrepancy in magnitude (but not in shape), is found. Another is when the present data are plotted as a function of target Z, the cross sections decrease in going from nitrogen to neon but increase from nitrogen to argon. Additional experimental work would be required to answer this question. But, the reader is reminded that our observations about the impact energy dependence, projectile charge state dependence, and scaling with ionization potentials are all unaffected by possible underestimations in magnitude in the neon target cross sections.

ACKNOWLEDGMENTS

This work was supported by the U.S. Department of Energy, Grant Nos. ER54578 and ER53175. A.C.F.S. is grateful for support obtained from the CNPq (Brazil).

[1] E. Rutherford, Philos. Mag. **47**, 277 (1924).
[2] H.H. Lo and W.L. Fite, At. Data **1**, 305 (1970).
[3] R.C. Dehmel, H.K. Chau, and H.H. Fleischmann, At. Data **5**, 231 (1973).
[4] H.A. Scott *et al.*, Phys. Rev. A **18**, 2459 (1978).
[5] W. Erb, GSI Report No. P-7-78, 1978 (unpublished); W. Erb and B. Franske, GSI Report No. J-1-78, 1978 (unpublished).
[6] H. Knudsen *et al.*, Phys. Rev. A **19**, 1029 (1979).
[7] H. Tawara, T. Kato, and Y. Nakai, At. Data Nucl. Data Tables **32**, 235 (1985).
[8] G.D. Alton *et al.*, Phys. Rev. A **23**, 1073 (1981).
[9] K.H. Berkner, W.G. Graham, R.V. Pyle, A.S. Schlachter, and J.W. Stearns, Phys. Rev. A **23**, 2891 (1981).
[10] A.S. Schlachter *et al.*, Phys. Scr. T **3**, 153 (1983).
[11] S.A. Boman, E.M. Bernstein, and J.A. Tanis, Phys. Rev. A **39**, 4423 (1989).
[12] P.H. Mokler, Th. Stöhlker, R. Buttner, and K.-H. Schartner, Nucl. Instrum. Methods Phys. Res. B **83**, 37 (1993).
[13] O. Heber *et al.*, Phys. Rev. A **52**, 4578 (1995).
[14] W.S. Melo, M.M. Sant'Anna, A.C.F. Santos, G.M. Sigaud, and E.C. Montenegro, Phys. Rev. A **60**, 1124 (1999).
[15] R.E. Olson, R.L. Watson, V. Horvat, and K.E. Zaharakis, J. Phys. B **35**, 1893 (2002).
[16] D. Bates and G. Griffing, Proc. Phys. Soc., London, Sect. A **66**, 961 (1953); **67**, 663 (1954); **68**, 90 (1955).
[17] N. Bohr, Mat. Fys. Medd. K. Dan. Vidensk. Selsk. **18**, 1 (1948).
[18] E.C. Montenegro and W. Meyerhof, Phys. Rev. A **46**, 5506 (1992).
[19] V.P. Shevelko, D. Böhne, and Th. Stöhlker, Nucl. Instrum. Methods Phys. Res. A **415**, 609 (1998).
[20] V.P. Shevelko, O. Brnzanescu, W. Jacoby, M. Rau, and Th. Stöhlker, Hyperfine Interact. **114**, 289 (1998).
[21] V.P. Shevelko, I.Yu. Tolstikhina, and Th. Stöhlker, Nucl. Instrum. Methods Phys. Res. B **184**, 295 (2001).
[22] R.E. Olson, Nucl. Instrum. Methods Phys. Res. A **464**, 93 (2001).
[23] See the Lawrence Berkeley Laboratory heavy-ion fusion homepage website http:/www-hifar.lbl.gov/HIFhomepage/hithome.html
[24] See the GSI future project website http:/www-new.gsi.de/zukunftsprojekt/index_e.html
[25] D. Mueller, L. Grisham, I. Kaganovich, R.L. Watson, V. Horvat, K.E. Zaharakis, and Y. Peng, Princeton Plasma Physics Laboratory Report No. PPPL-3713, 2002 (unpublished).
[26] H. Knudsen, L.H. Andersen, H.K. Haugen, and P. Hvelplund, Phys. Scr. **26**, 132 (1982).
[27] Y. Nakai, A. Kikuchi, T. Shirai, and M. Sataka, JAERI-M Report No. 84-069, 1984 (unpublished).
[28] R.D. DuBois, Phys. Rev. A **36**, 2585 (1987).
[29] H. Atan, W. Steckelmacher, and M.W. Lucas, J. Phys. B **24**, 2559 (1991).
[30] M.M. Sant'Anna, W.S. Melo, A.C.F. Santos, G.M. Sigaud, and E.C. Montenegro, Nucl. Instrum. Methods Phys. Res. B **99**, 46 (1995).
[31] R.D. DuBois and L.H. Toburen, Phys. Rev. A **38**, 3960 (1988).
[32] B.L. Schram, Physica (Amsterdam) **32**, 197 (1966).
[33] A. Müller, K. Huber, K. Tinschert, R. Becker, and E. Salzborn, J. Phys. B **18**, 2993 (1985).